Monthly Notices
of the
ROYAL ASTRONOMICAL SOCIETY
MNRAS **456,** 192–206 (2016) doi:10.1093/mnras/stv2611

Antarctica photometry of the Blazhko RR Lyrae star S Arae

C. Zalian,* M. Chadid, J. Vernin, L. Abe and A. Agabi
Université Nice Sophia-Antipolis, Observatoire de la Côte d'Azur, UMR 7293, Parc Valrose, F-06108 Nice Cedex 02, France

Accepted 2015 November 3. Received 2015 November 3; in original form 2015 May 3

ABSTRACT

We pursue the study of S Arae, an RRab Lyrae Blazho star, using unique, uninterrupted and accurate optical photometric data acquired from Antarctica at Dome C by PAIX – Photometer AntarctIca eXtraction – during 150 d. The PAIX data were analysed using both Period04 and PDM13. Besides a main pulsation period of 0.452 d and a modulation period of 47.264 d, three other significant frequencies were found. Multiplet patterns, up to the ninth order, were also extracted, showing a clear asymmetric structure. Following these results, a new approximation of the main-frequency harmonics amplitude decrease is suggested, replacing the usual exponential fit by a hyperbolic one. The physical properties of the Blazhko star, namely metallicity, temperature, mass, were obtained using a new approach based on the study of these parameters for each Blazhko phase. Finally, the PAIX data reveal a residual scatter that occurs during a small phase interval, 10 per cent of the pulsation period, corresponding to the phase of the main shock passage across the atmosphere. The position of the so-called main bump, corresponding to the shock resulting from the infalling atmosphere and the expanding photosphere, varies from one cycle to another and, moreover, around this main bump, two other bumps appear and vanish at different phases during a Blazhko cycle. Following these observations, we discuss the relation between the bump topology and the Blazhko period and give new insights for future Blazhko theoretical investigations.

Key words: shock waves – methods: observational – techniques: photometric – stars: atmospheres – stars: oscillations – stars: variables: RR Lyrae.

1 INTRODUCTION

Since their discovery at the end of the 19th century, RR Lyrae stars have contributed to almost every branch of astronomy, from chemical and dynamical properties of old stellar populations to distance measurements. These pulsating horizontal branch A-F stars, with period ranging from 0.2 to 1.2 d are relatively low-mass, metal poor Population II stars with an average absolute magnitude of 0.75 and commonly found in globular clusters.

In 1907, Russian astronomer Sergey Nikolaevich Blazhko observed an amplitude modulation of the periodic pulsation of a RR Lyrae-type star, RW Dra (Blazko 1907). This phenomenon, now known as the Blazhko effect, has been since observed in many others: RRab, RRc and recently in RRd-type star. However, none of the dozens of existing models managed to describe fully the whys and wherefores of this amplitude and period modulation. Amongst these, three are considered as the most cogent: Shibahashi magnetic model (Shibahashi 2000), Nowakowski and Dziembowski resonance mechanism (Nowakowski & Dziembowski 2001) and Stothers' convective model (Stothers 2006). Still, none are entirely satisfactory. The magnetic oblique rotator mechanism proposed by Shibahashi has been ruled out by Chadid et al. (2004) due to the absence of the required 1-kG strong magnetic field. The asymmetric structured spectrum observed in Blazhko stars (Chadid & Chapellier 2006) undermines the resonance models, based on a non-linear resonant coupling between the dominant radial mode, and non-radial models. Finally, the model suggested by Stothers, based on a periodic change in the turbulent convective properties of the star, has also been dismissed by Molnár, Kolláth & Szabó (2012) due to its incapability to explain strong modulation in short time-scale. Recently, the possibility of an unstable resonant interaction between the fundamental and the ninth radial overtone has been suggested as a new paradigm for the Blazhko effect (Buchler & Kolláth 2011; Szabó 2014).

Another ongoing matter of study on RRab-type stars is the presence of shock waves in their atmosphere. Hill (1972) showed that the so-called bump and hump in the light curve of these stars are a consequence of two shock waves propagating through their atmosphere. The κ and γ mechanisms are responsible for the main shock occurring just before the maximum of the light curve, while the one occurring just before the minimum would be caused by the collision of the infalling upper atmosphere with the expanding photosphere. Chadid et al. (2014) have shown that this description was incomplete as other bumps can be observed in the light curve of S Arae, and would be, thus, evidence of other shocks. They have also

* E-mail: cyruszalian@gmail.com

proposed a new explanation for the Blazhko effect based on the idea that the multishock structure develops a stationary coronal structure that drives an outflowing wind (Stellingwerf 2013) which could possibly explain the observed modulation. The bump phenomenon is indubitably linked to the Blazhko effect, whether as a cause or as a consequence of the mechanism. Following Hertzsprung's work on the link between the bump phase and the pulsation period of Cepheid stars (Hertzsprung 1926), Guggenberger & Kolenberg (2006) have suggested that a similar result could be computed for RR Lyrae stars. Unlike Cepheids stars where the bump position does not vary from one period to another for a given star, RR Lyrae bumps do move from one pulsational cycle to another. This phase variation can be linked to the Blazhko cycle and thus may explain the modulation observed or be a consequence of it.

Frequency analysis of RR Lyrae light curve, based on Fourier decomposition, is of primary importance when it comes to understand the oscillatory behaviour of the star. Empirical surveys and theoretical studies have shown that the physical characteristics of RR Lyrae stars can be deduced from their Fourier analysis. Indeed, metallicity, absolute magnitude, distance, temperature, luminosity, surface gravity and mass can be computed using as few parameters as the visual amplitude, the rise time, the main period and the Fourier parameter A_1, A_3 and ϕ_{31} (Nemec 2011). However, these equations do not apply well to Blazhko-type stars, due to the continuous variation of their input parameters. Different approaches have been considered to tackle such an issue. The most widespread one consists in taking the averaged value as in Feast et al. (2008). Unfortunately, this method leads to unreliable results as shown by Nemec et al. (2013). The latter suggested that the overall averaged values should be replaced by an average of instant values. However, this implies, first, that the equations for physical properties work for each Blazhko phase and, moreover, have a high-resolution coverage on the total time span with few gaps as, for instance, in the data acquired by *CoRoT* and *Kepler*.

This paper follows the first 49-d photometric study of the RR Lyrae Blazhko star S Arae (Chadid et al. 2010b). New observations include three Blazhko periods of S Arae with a time span of over 150 d. Section 2 will present the observation protocol together with the frequency extraction process. The following section features the computation results, including the light-curve modulation multiplet and the study of its asymmetric structure, the analysis of the harmonic amplitude decrease, the possibility of period-doubling and the presence of non-radial mode and overtones. In this same section, the evolution of parameters such as the rise time, the Fourier coefficients, the maximum amplitude-phase during a Blazhko cycle is also investigated together with an Observed-minus-Calculated (O−C) analysis. In Section 4, we use the results obtained in the previous paragraph to compute the physical characteristics of S Arae, namely, its metallicity, temperature, absolute magnitude, mass, luminosity, etc. To obtain such results, we follow a new approach avoiding the hurdle of averaged input parameters which leads to unreliable results in the case of Blazhko stars. Finally, we close our discussion with an analysis of bumps topology, and thus shock waves, in S Arae.

2 OBSERVATIONS AND TOOLS

2.1 PAIX photometry

The photometric data were acquired at Dome C on the Antarctica plateau using PAIX – Photometer AntarctIca eXtraction – attached to a 40-cm Ritchey–Chretien f/10 telescope. More details on the setup and design of PAIX can be found in Chadid et al. (2010b). An almost continuous acquisition of photometric observations during 150 nights – from 2009 April 18 until September 20, with a 65 per cent duty cycle – is presented (Fig. 1) covering almost three Blazhko period. S Arae *V*-magnitude varies from 9.79 to 11.14 mag (1.35 mag amplitude) with a 0.452 d period. A strong amplitude modulation of a 48.544 d period is also observable.

2.2 Frequency analysis *via* PDM13 and Period04

A frequency analysis of the photometric data was performed using Period04 (Lenz & Breger 2005) and PDM13 (Zalian, Chadid & Stellingwerf 2014, https://forge.oca.eu/trac/PDM13). While Period04 relies on a Fourier-based analysis, as it fits an harmonic model function to the data, PDM13 does not assume an a priori model for the photometric function.

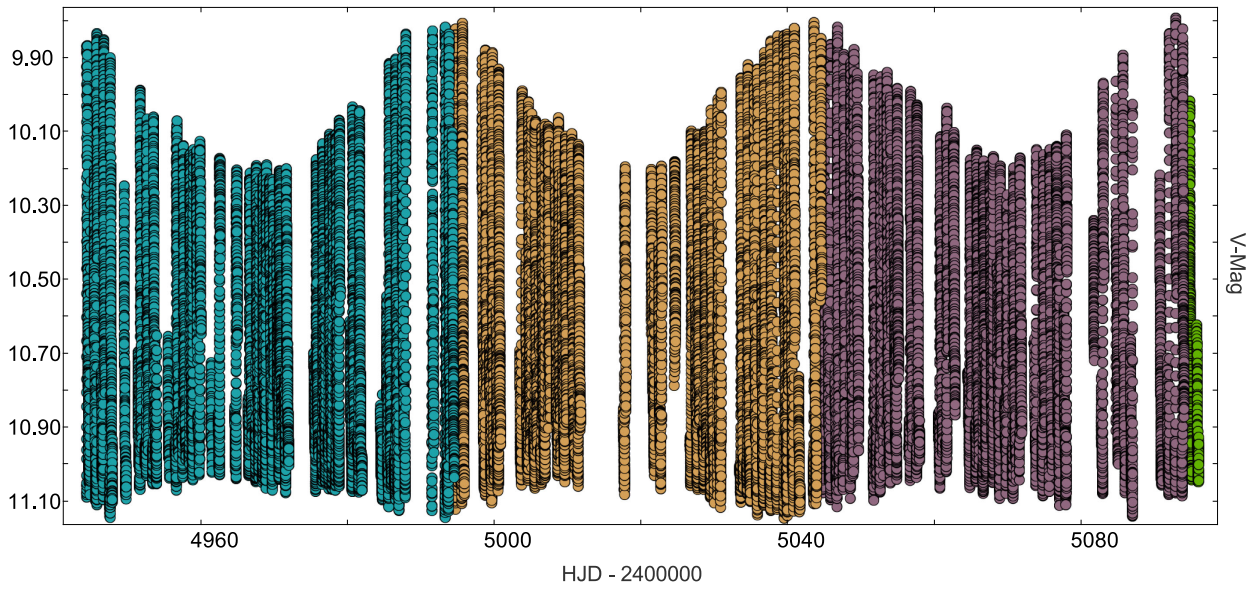

Figure 1. PAIX light curve of the Blazhko star S Arae over one polar night (150 d).

PDM13 is based on Stellingwerf's phase dispersion minimization (PDM) technique (Stellingwerf 1978). As shown by its author (Stellingwerf 2011), PDM outmatches existing algorithms in several cases and is particularly efficient for poor long spanned data – i.e. few data with large gaps for extended time-scale.

Besides, numerous significance test studies were conceived for the PDM technique. Amongst these, the β function test (Schwarzenberg-Czerny 1997) and the Monte Carlo test by Linnell Nemec & Nemec (1985) were implemented in PDM13 allowing more reliable extractions of frequencies.

Unlike existing programs where residuals are calculated by prewhitening a prominent frequency, PDM performs a mean curve pre-whitening, allowing a different approach to the light-curve frequency analysis. This is particularly interesting when it comes to the study of transitory effect as we will see in the discussion below.

Finally, combining these two tools, Period04 and PDM13, allows us to obtain more reliable results. Indeed, as the data structure presents several gaps, bias frequencies – aliases – can emerge. One of PDM13 main features is the ability to dodge such an issue using the *Auto-segmentation* feature. This option, originally based on the Lee and Heghinian test (Lee & Heghinian 1977), was lately improved to give faster and more accurate results. It computes the average time difference $\overline{\mathrm{d}t}$ between each photometric point as well as the standard deviation σ. The 50 or 95 per cent confidence level is then given by

$$[\overline{\mathrm{d}t} - i\sigma; \overline{\mathrm{d}t} + i\sigma], \quad (1)$$

with $i = 1$ or 2 for, respectively, the 50 and 95 per cent confidence level. A time span between two points larger than the one included in this confidence interval can then be considered as a gap.

3 ANALYSIS AND RESULTS

3.1 Fourier analysis of the full data set

First, we performed a Fourier analysis of the complete data set. The goal was to obtain a first overall picture of S Arae with its main and modulation period in term of mean values. Indeed, as we will see in Section 3.2, those parameters, along with others, vary over time. Still, these mean coefficients, and those derived from them, are necessary to compute the fundamental characteristics of the star.

A significance test was performed using the signal-to-noise ratio criteria with Period04 and the Monte Carlo test with PDM13 for each frequency extracted. Only those showing positive results for each test were kept (see Fig. 2).

Fig. 3 shows the evolution of the frequency spectrum along the extraction process. We were able to extract 85 significant frequencies. We found a main frequency of 2.213 02 d^{-1} with a $\sigma_f = 1.485 \times 10^{-6}\,\mathrm{d}^{-1}$ and its harmonics up to the 22th order; a modulation frequency of 0.0211 d^{-1} with a $\sigma_{f_\mathrm{b}} = 2.405 \times 10^{-5}\,\mathrm{d}^{-1}$ and its second harmonic together with Blazhko multiplet structure. Additional frequencies will be addressed later on in this paper (Section 3.1.5)

The Fourier parameters needed to compute physical characteristics are presented in Table 1. Epoch-independent phase differences and amplitude ratios are, respectively, given by the following formulae: $\phi_{i1} = \phi_i - i\phi_1$ and $R_{i1} = A_k/A_1$ (Simon & Lee 1981).

3.1.1 Multiplet structure

The frequency spectrum S Arae includes Blazhko triplet to undecaplet structure, suggesting a non-linear modulation. The map of harmonics, Fig. 4, shows an irregular pattern. Components were detected up to the undecaplet order on the left-hand side, while on the right-hand side, in most cases, only one side peak could be found. For each harmonic, the positive side peak shows lower amplitude than negative one, resulting in a clear asymmetry in the map of harmonics. Fig. 5 corroborates our assessment as negative sides are more prominent than the positive one in this close-up look of the original spectrum around the ninth harmonic. This is particularly interesting as three-fourths of the known Blazhko stars show the opposite behaviour (Alcock 2003). Still, focusing on the triplet structure, the positive frequency side have, indeed, a higher amplitude than the negative for almost all harmonics.

3.1.2 Harmonics deviation

Theoretically, sidelobes in the Fourier spectrum of a modulated signal will be equidistant to the carrier main frequency and harmonics. However, a non-negligible proportion of Blazhko stars present a sidelobe frequency offset (Alcock 2003). For each mutliplet order, we have computed the average harmonic deviation δf as given by equation (2) (the results are summarized in Table 2):

$$\delta f_i = \frac{\sum_{n=1}^{k} f_{n+ib} + f_{n-ib} - 2 \times f_n}{k}. \quad (2)$$

Due to the limitation of our results, we can only draw conclusions for the triplet and quintuplet structures. The first one shows a negligible frequency offset of 0.000 11 d^{-1} falling in the $\pm 0.0002\,\mathrm{d}^{-1}$ interval observed by Alcock in all Blazhko stars. The latter one however shows a stronger asymmetry. Still, this has to be balanced by

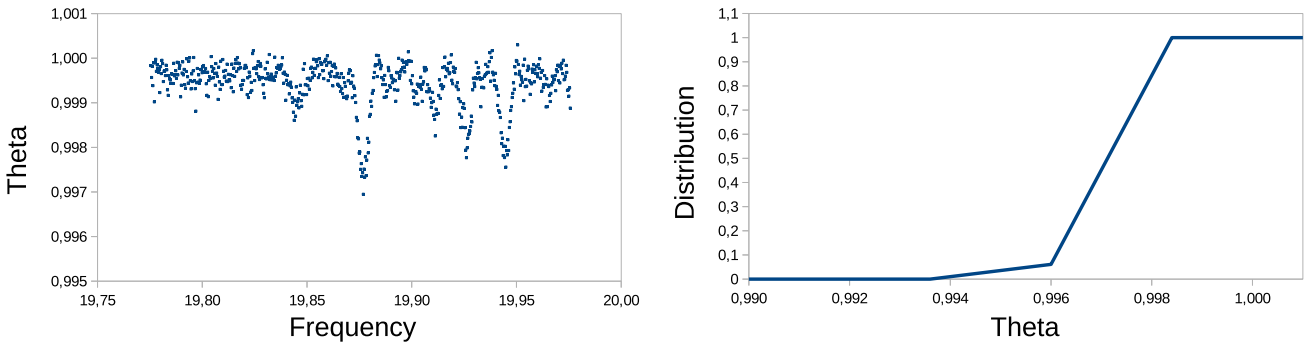

Figure 2. Significance test using the Monte Carlo method from PDM13 for $9f_0 - 2f_\mathrm{b}$. The left figure represents the result of the frequency analysis. The minimum value of theta, 0.9968, is reached for a frequency corresponding to $9f_0 - 2f_\mathrm{b}$. The right figure represents the theta distribution. For theta = 0.9968 the distribution is above the 0.1 value, hence the result was disregarded.

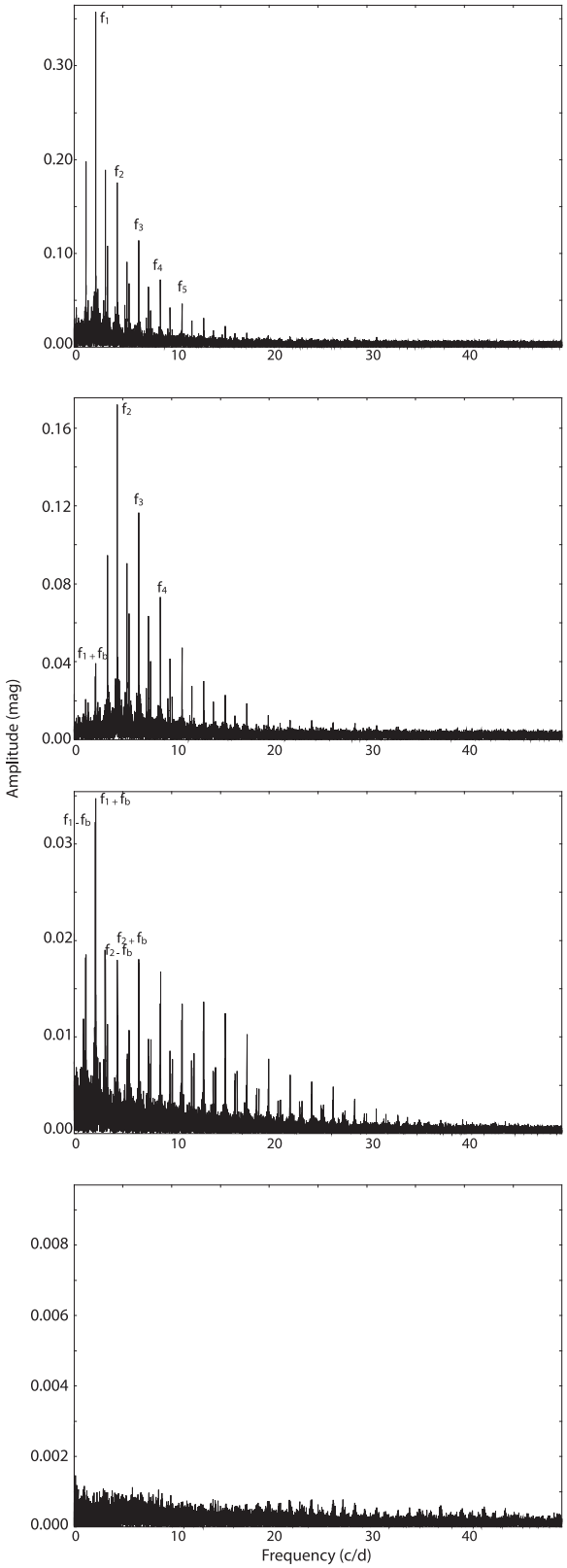

Figure 3. Frequency spectrum of S Arae for different pre-whitening steps. From top to bottom: original data spectrum; spectrum after pre-whitening with the main frequency; spectrum from the signal pre-whitened with the main frequency and its harmonics; spectrum after all significant frequencies have been pre-whitened.

Table 1. Epoch-independent Fourier parameters for S Arae.

A_1 (mag)	R_{21}	R_{31}	ϕ_{21} (rad)	ϕ_{31} (rad)
0.36	0.479	0.327	2.084	4.065

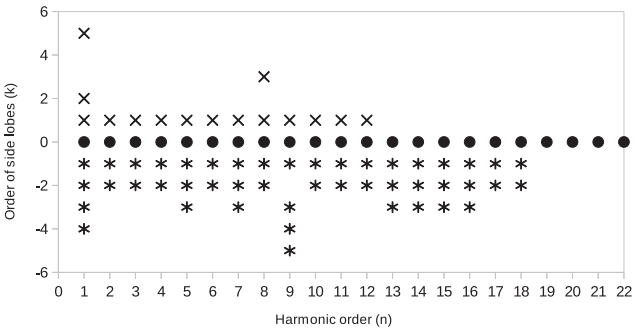

Figure 4. Map of harmonics and side peaks in the frequency spectrum of S Arae.

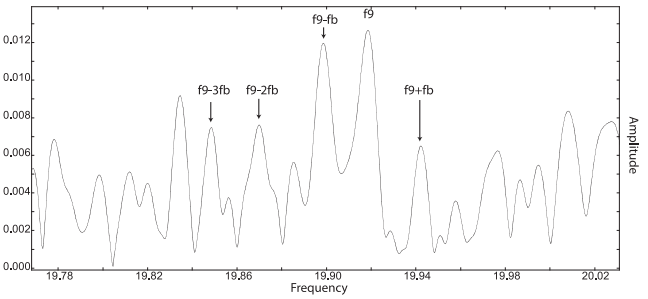

Figure 5. Original Fourier spectrum around the ninth harmonic.

Table 2. Multiplet structures, degree of deviation and degree of asymmetry.

Multiplet	No. of freq.	δf (d^{-1})	$Q - \overline{Q}$
Triplet	30	0.000 11	0.002 29
Quintuplet	18	− 0.004 04	0.017 93

the unequilibrated distribution of the sidelobes (17 right sidelobes for one left sidelobe).

To verify this observation, we have fixed all sidelobes to their theoretical value, namely $kf_0 \pm nf_b$, and then ran a least-squares fitting algorithm where all frequencies, amplitudes and phases were defined as degrees of liberty. No differences were observed with the results already computed with the frequency extraction algorithm.

The reason for such discrepancy is still unknown. It can be caused by the omission of frequencies or by cycle to cycle changes as we will see in Section 3.2. However, as shown by Alcock, this offset cannot be explained only by noise or measurement uncertainty.

3.1.3 Amplitude of the harmonics

It is generally admitted that the harmonic/main-frequency amplitude ratio follows an exponential variation along the harmonic order. However, when it comes to high orders, the corresponding point fails to comply with this scenario (Chadid et al. 2010a). A hyperbolic fit

seems more appropriate (Fig. 6). Fitting these amplitudes with the function given in equation (3) gave the best approximation of the spectrum shape for the main frequency and its harmonics – standard deviation of $\sigma_y = 0.003$:

$$A(f) = a_1 \times f + a_0 + \frac{a_{-1}}{f} + \frac{a_{-2}}{f^2}, \quad (3)$$

with $a_1 = 0.7$ mmag d, $a_0 = -0.059$ mag, $a_{-1} = 1.16$ mag d^{-1} and $a_{-2} = -0.54$ mag d^{-2}. The fit is represented in Fig. 7.

The other amplitude ratio corresponding to higher harmonics multiplets are presented in Fig. 6. As underlined by Jurcsik et al. (2005), these ratios tend to decrease less rapidly than the main component one. Left sidelobes follow a quasi-exponential decrease, except for the second harmonic which presents an unexpected low value. Right sidelobes do not follow a similar clear path as two standstills precede the exponential decrease – which vanishes for the higher orders.

3.1.4 Multiplet amplitude asymmetry

The degree of asymmetry in the modulation amplitudes $Q - \overline{Q}$ computes the average amplitude offset:

$$Q - \overline{Q}_i = \frac{\sum_{n=1}^{k} \frac{A_{ni+} - A_{ni-}}{A_{ni+} + A_{ni-}}}{k}. \quad (4)$$

Fig. 6 shows that the modulation amplitude of the higher frequency side of the quintuplet structure is larger than its lower frequency counterpart ($Q - \overline{Q} = 0.0179$). This indicates a higher than average asymmetry to the right. While the triplet structure demonstrates that the modulation amplitude of the higher and lower frequencies is almost equal ($Q - \overline{Q} = 0.0023$).

These results, combined with those seen in Section 3.1.1, where negative multiplet components are more prominent than positive one, go against what is normally expected (see for instance Chadid et al. 2010a). However, as shown by Benkő, Szabó & Paparó (2011), the asymmetry depends on the relative phase of the amplitude and phase modulation; hence, both left and right asymmetries can be expected a priori.

3.1.5 Additional frequencies: radial overtones and non-radial pulsation

Besides the main frequency, its harmonics and the Blazhko multiplet, other frequencies were detected. After withdrawing those corresponding to aliases, we found a first one at 3.1308 d^{-1} with a 2.40 mmag amplitude corresponding to a possible first overtone. Combination with the main frequency $f_0 + f_N$ (see Table 3) confirms that the additional signal is not introduced by a possible background star. Still, its frequency ratio with the fundamental $f_N/f_0 = 0.707$ comes as very low compared to the canonical value of 0.74–0.75. Moreover, Guggenberger et al. (2012) and Chadid et al. (2010a) have found similar value, respectively, 0.703 and 0.696 in V445 Lyr and V1127 Aql and both argued for a non-radial pulsation frequency. Indeed, extremely high metallicity value would be needed according to models (Popielski, Dziembowski & Cassisi 2000; Szabó, Kolláth & Buchler 2004; Smolec & Moskalik 2008) to reach such a low ratio. Section 4 will show that the required abundance was not found. All in all, f_N is most likely to be a non-radial mode as suggested by the non-adiabatic non-radial calculations presented by Van Hoolst, Dziembowski & Kawaler (1998) and in Dziembowski & Cassisi (1999) model.

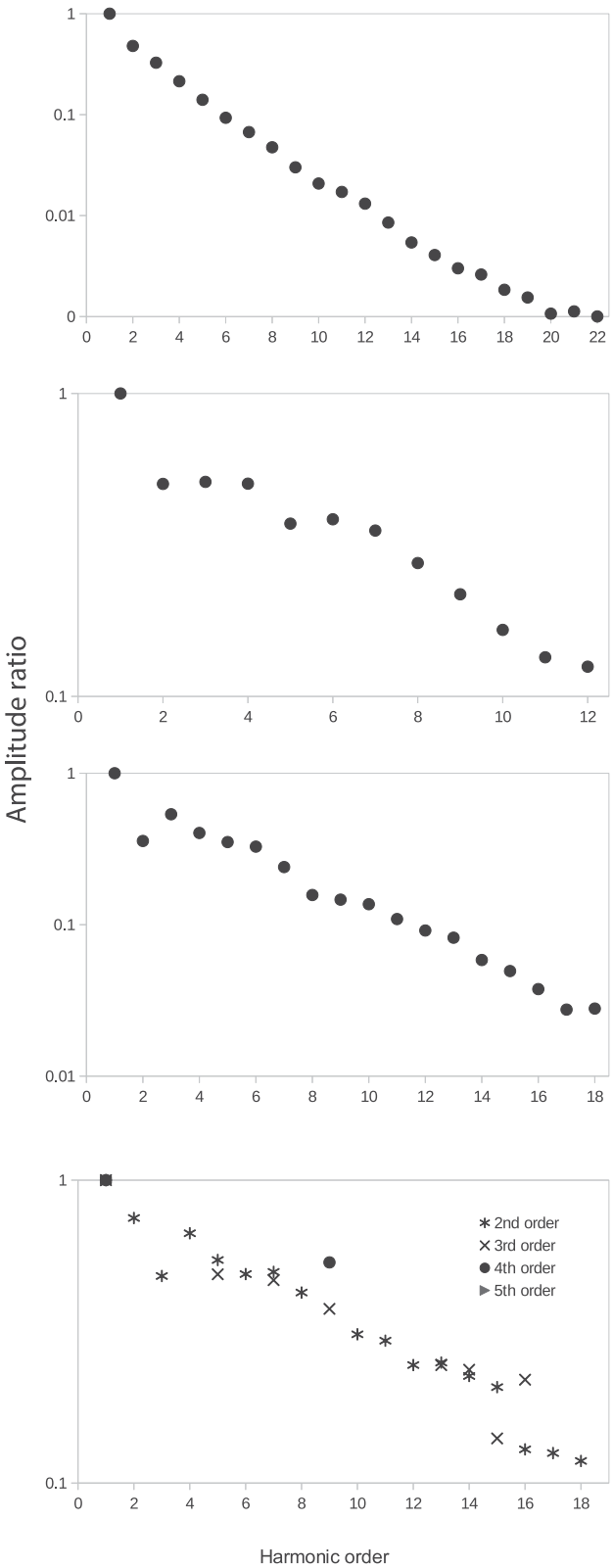

Figure 6. From top to bottom: amplitude ratio of the harmonic components A_{nf_0}/A_{f_0}; amplitude ratio of the right modulation component $A_{nf_0+f_b}/A_{f_0+f_b}$; amplitude ratio of the left modulation component $A_{nf_0-f_b}/A_{f_0-f_b}$; amplitude ratio of the harmonic components $A_{nf_0-kf_b}/A_{f_0-kf_b}$ with k being the multiplet order.

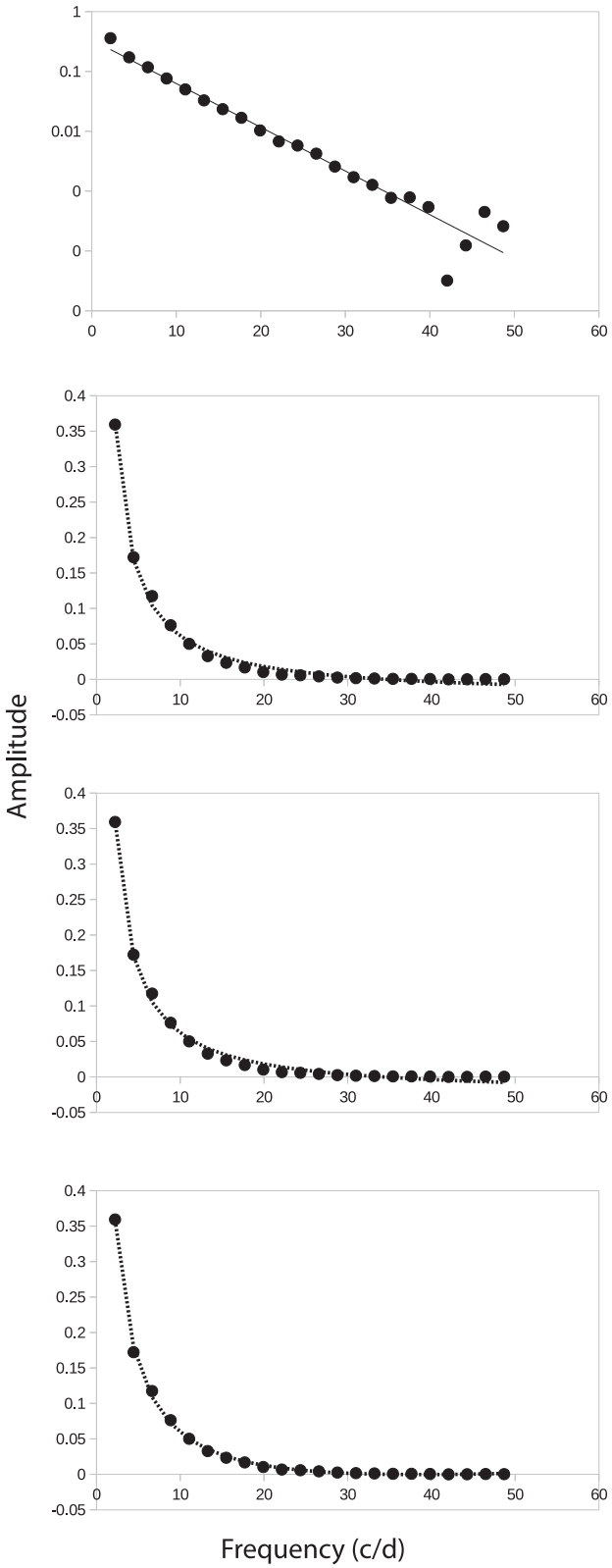

Figure 7. Fourier spectrum for the main period and its harmonics (dots) and fitting function. From top to bottom: exponential fit in a log scale; $\frac{a_{-1}}{f}$ fit; $\frac{a_{-1}}{f} + \frac{a_{-2}}{f^2}$ fit; $a_1 \times f + a_0 + \frac{a_{-1}}{f} + \frac{a_{-2}}{f^2}$ fit.

Table 3. Additional frequencies and combinations.

	Frequency (d^{-1})	Amplitude (mmag)
f_N	3.1309	2.48
$f_N + f_0$	5.3516	1.41
$f_N - f_0$	0.9134	3.78
$f_{N'}$	2.9571	2.09
$f_{N'} - f_0$	0.7479	3.26
f_2	3.8018	2.40
$f_2 + f_0$	6.0077	1.55
$f_2 + f_0 + f_b$	6.0308	1.47
$f_2 - f_0$	1.5904	1.69

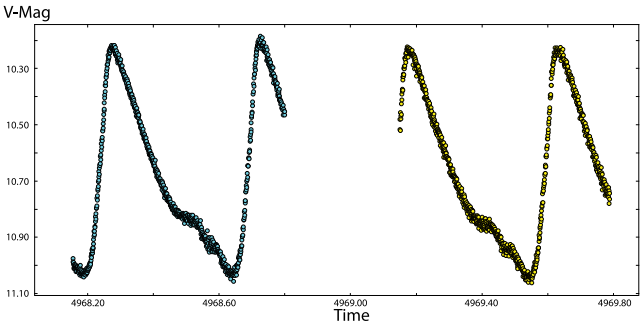

Figure 8. Four consecutive periods of S Arae light curve showing possible evidence of period doubling.

Similarly, we have found a 2.10-mmag amplitude peak at 2.9571 d^{-1}, which, with a frequency ratio $f_0/f_{N'} = 0.748$ does fall in the usual first overtone interval. However, once again, this would imply a metallicity $Z = 10^{-4}$ that does not match the one found in Section 4.

The third remaining peak in the Fourier spectrum is at 3.8018 d^{-1} with a 2.40 mmag amplitude. Its frequency ratio with f_0, $f_0/f_2 = 0.582$, suggests a second overtone period. Similar ratios were reported for several RR Lyrae stars (Jurcsik et al. 2008; Chadid et al. 2010a; Poretti et al. 2010). Combinations with the fundamental and its triplet structure were also found (Table 3).

The light curve of S Arae shows apparent evidence of period doubling (Fig. 8). Still, none of the expected half-integer multiples of the fundamental mode (Szabó 2010) were extracted, thus preventing us from any conclusion on this mechanism.

All in all, nine additional frequencies and their combination with the fundamental period were found (Table 3). Together with the initial 85 frequencies corresponding to the main frequency, its harmonics and their multiplet structure, we obtained 94 significant frequencies along this extraction process (Tables 4–7).

3.2 Blazhko modulation and cycle-to-cycle variation

The amplitude and phase modulation behaviour can be clearly seen in the folded light curve with the main pulsation period (Fig. 9). The Blazhko effect appears also in the frequency spectrum as sidelobes to the main frequency and its harmonics, as shown in Fig. 10 inner panel and in Table 6. The multiplet structure goes from triplet to nonuplet, suggesting a non-linear modulation. Finally, it is interesting to observe that not only the amplitude but also the shape and the period vary during the Blazhko cycle (Fig. 11).

Table 4. Fourier amplitudes, phases and identification(s) for the PAIX data of the star S Arae.

ID	Frequency (c d^{-1})	Amplitude (mag)	Phase (cycles)
Main frequency and harmonics			
f_1	2.213 027 1687	0.360 500 5238	0.724 230 5549
$2f_1$	4.426 062 7971	0.172 758 7355	0.780 228 0473
$3f_1$	6.639 109 7894	0.117 885 2429	0.819 898 4413
$4f_1$	8.852 175 6243	0.077 234 6143	0.777 843 7932
$5f_1$	11.065 220 1741	0.050 612 3324	0.840 764 3425
$6f_1$	13.278 315 6948	0.033 568 1872	0.639 492 9331
$7f_1$	15.491 367 8143	0.024 217 2065	0.657 329 851
$8f_1$	17.704 399 0995	0.017 129 7428	0.788 505 6269
$9f_1$	19.917 569 1613	0.010 841 2851	0.209 208 6861
$10f_1$	22.130 840 637	0.007 490 495	0.113 848 5242
$11f_1$	24.343 808 5216	0.006 181 2056	0.543 557 3695
$12f_1$	26.556 856 2969	0.004 733 343	0.588 446 7506
$13f_1$	28.769 821 2115	0.003 074 8479	0.073 781 1655
$14f_1$	30.982 911 9028	0.001 952 8045	0.883 086 0946
$15f_1$	33.194 618 5192	0.001 466 0497	0.600 535 7479
$16f_1$	35.408 820 9889	0.001 083 3996	0.854 055 2134
$17f_1$	37.621 329 8894	0.000 940 1252	0.573 421 4576
$18f_1$	39.839 414 3299	0.000 664 0706	0.550 726 6563
$19f_1$	42.080 795 4777	0.000 556 7757	0.438 506 6574
$20f_1$	44.264 425 7766	0.000 385 1475	0.987 536 2732
$21f_1$	46.455 085 0014	0.000 405 492	0.878 810 4214
$22f_1$	48.525 817 5994	0.000 361 4866	0.657 530 5593

Table 5. Fourier amplitudes, phases and identification(s) for the PAIX data of the star S Arae.

ID	Frequency (c d^{-1})	Amplitude (mag)	Phase (cycles)
Blazhko modulation frequency			
f_b	0.021 159 4008	0.022 255 0213	0.706 543 2622
$2f_b$	0.037 047 6041	0.008 540 1675	0.348 732 3083

3.2.1 *Frequency analysis of the extracted envelope*

The maximum–minimum representation of the envelope (Fig. 12) shows a weak non-sinusoidal shape. This observation is confirmed by the frequency analysis. For the upper part of the modulation we obtained two significant values $f_{m_{up_1}} = 0.0196\,\mathrm{d}^{-1}$ and $f_{m_{up_2}} = 0.0437\,\mathrm{d}^{-1}$ with respective amplitude of 0.11 mag and 0.02 mag. For the lower part of the modulation we obtained one significant value $f_{m_{low}} = 0.0207\,\mathrm{d}^{-1}$ with a 0.03 mag amplitude (Fig. 13). The maximum pulsation amplitude is 1.13 mag, while the minimum pulsation amplitude is 0.75 mag, hence a 0.38-mag modulation amplitude. It is interesting to see that there is also a phase lag in the maximum–minimum envelope (Fig. 12) and a significant difference in amplitude between these two.

3.2.2 *Loop diagrams*

The maximum magnitude–maximum phase diagram, also known as the loop diagram, is represented in Fig. 14 (standard deviation: $< \theta_{\mathrm{Maxmag}} > = 0.011$, $< \theta_{\mathrm{Maxphase}} > = 0.002$). We can clearly see the amplitude and phase modulation occurring in S Arae and the phasing between each contribution. The three cycles present a similar behaviour, following a very similar path every time with a phase offset between each. For each Blazhko cycle, when reaching maximum magnitude, the phase at maximum magnitude tends to stop varying for a couple of pulsation period. This phenomenon is represented by a small loop, in the upper-right part of each path.

Table 6. Fourier amplitudes, phases and identification(s) for the PAIX data of the star S Arae.

ID	Frequency (c d^{-1})	Amplitude (mag)	Phase (cycles)
Modulation multiplet frequencies			
f_1+f_b	2.232 900 4771	0.035 780 2844	0.586 231 4704
f_1-f_b	2.193 564 3836	0.034 766 2369	0.986 598 6112
f_1+2f_b	2.250 646 6871	0.004 442 1198	0.295 167 1724
f_1-2f_b	2.171 367 393	0.006 321 2977	0.575 509 4678
f_1-3f_b	2.1467 896 249	0.003 464 9381	0.776 320 6172
f_1-4f_b	2.126 246 6078	0.002 429 1243	0.344 384 9401
f_1+5f_b	2.313 140 4601	0.002 554 967	0.351 485 4465
$2f_1+f_b$	4.445 727 4109	0.017 991 809	0.739 445 1549
$2f_1-f_b$	4.407 738 446	0.012 416 2054	0.356 866 9901
$2f_1-2f_b$	4.383 723 4551	0.004 740 2109	0.186 254 9455
$3f_1+f_b$	6.659 184 0836	0.018 272 736	0.571 740 0266
$3f_1-f_b$	6.619 189 0799	0.018 635 6428	0.240 481 496
$3f_1-2f_b$	6.598 002 5466	0.003 050 3398	0.994 056 0718
$4f_1+f_b$	8.872 081 84	0.018 025 8166	0.404 747 1838
$4f_1-f_b$	8.832 591 227	0.014 022 5865	0.566 383 2269
$4f_1-2f_b$	8.810 145 1307	0.004 221 3581	0.581 067 5732
$5f_1+f_b$	11.085 130 2619	0.013 304 5542	0.432 170 3268
$5f_1-f_b$	11.045 433 7957	0.012 212 7944	0.607 787 4899
$5f_1-2f_b$	11.0239 124 098	0.003 445 0476	0.043 133 9187
$5f_1-3f_b$	11.003 258 3123	0.001 693 8707	0.200 360 0678
$6f_1+f_b$	13.298 000 8263	0.013 749 8553	0.342 912 8454
$6f_1-f_b$	13.258 558 2541	0.011 394 0786	0.299 638 8463
$6f_1-2f_b$	13.237 241 3466	0.003 095 8103	0.634 467 9856
$7f_1+f_b$	15.511 044 3739	0.012 620 2208	0.431 299 286
$7f_1-f_b$	15.471 977 248	0.008 352 3707	0.507 557 9617
$7f_1-2f_b$	15.450 788 8674	0.003 146 9833	0.201 363 2312
$7f_1-3f_b$	15.431 824 2127	0.001 620 0099	0.873 562 4247
$8f_1+f_b$	17.724 310 7807	0.009 855 297	0.395 407 6652
$8f_1-f_b$	17.685 077 6469	0.005 460 6614	0.256 147 9434
$8f_1-2f_b$	17.664 517 5543	0.002 690 2524	0.859 722 1007
$8f_1+3f_b$	17.765 642 4013	0.001 124 0333	0.643 795 7477
$9f_1+f_b$	19.937 273 6521	0.007 773 3786	0.875 191 8044
$9f_1-f_b$	19.897 996 7913	0.005 088 9469	0.921 781 0191
$9f_1-3f_b$	19.856 537 2434	0.001 302 6213	0.897 864 4052
$9f_1-4f_b$	19.836 079 4681	0.001 299 7758	0.117 014 5476
$9f_1-5f_b$	19.815 191 4123	0.000 904 4227	0.351 395 988

3.2.3 *Fourier parameters*

The variation of Fourier parameters describes the pulsation properties changes along the modulation cycle. As presented in Section 3.1, these are the amplitude ration $R_{k1} = A_k/A_1$ and the epoch-independent phase difference $\phi_{k1} = \phi_k - k\phi_1$. To compute these parameters, the artificial signal, created from the original one, was subdivided in 166 bins of 0.9 d, therefore containing two pulsation periods per bin. Using a short time-scale minimizes the influence of the Blazhko effect on our results. For each bin, a fit including the fundamental frequency and two harmonics was calculated. The results are displayed in Fig. 15. Average values of the parameters are given in Table 8 (phases are in radians).

First, the amplitude of the fundamental frequency presents a smooth sine variation with a perturbation at each cycle similar to the bump phenomenon observed in the light curve of S Arae (Chadid et al. 2014). Moreover, the perturbation position varies from one

Table 7. Fourier amplitudes, phases and identification(s) for the PAIX data of the star S Arae – part 2.

ID	Frequency (c d^{-1})	Amplitude (mag)	Phase (cycles)
Modulation multiplet frequencies part 2			
$10f_1+f_b$	22.150 108 1925	0.005 930 5667	0.966 207 2898
$10f_1-f_b$	22.110 734 3971	0.004 747 8656	0.525 927 1477
$10f_1-2f_b$	22.089 427 3552	0.001 958 3553	0.836 457 5368
$11f_1+f_b$	24.363 564 2973	0.004 815 2042	0.957 838 1881
$11f_1-f_b$	24.323 560 0367	0.003 789 2257	0.688 013 1141
$11f_1-2f_b$	24.302 656 6797	0.001 865 5965	0.999 617 6804
$12f_1+f_b$	26.576 523 3862	0.004 484 0993	0.431 858 7972
$12f_1-f_b$	26.536 576 2776	0.003 182 427	0.877 414 8929
$12f_1-2f_b$	26.514 975 9827	0.001 549 9824	0.708 301 9867
$13f_1-f_b$	28.748 484 6058	0.002 851 4518	0.662 702 8182
$13f_1-2f_b$	28.727 252 9558	0.001 579 0377	0.611 603 0758
$13f_1-3f_b$	28.708 701 6077	0.000 848 7763	0.244 276 3763
$14f_1-f_b$	30.962 020 3472	0.002 031 6767	0.252 104 7258
$14f_1-2f_b$	30.941 192 6478	0.001 426 4304	0.193 394 8853
$14f_1-3f_b$	30.922 345 0601	0.000 819 9416	0.271 623 1518
$15f_1-f_b$	33.175 458 8328	0.001 717 7029	0.336 527 4907
$15f_1-2f_b$	33.155 140 4299	0.001 310 3587	0.730 918 6119
$15f_1-3f_b$	33.134 526 543	0.000 486 5219	0.636 986 6012
$16f_1-f_b$	35.388 504 6425	0.001 305 3503	0.387 480 2719
$16f_1-2f_b$	35.366 042 2034	0.000 816 7886	0.488 909 4373
$16f_1-3f_b$	35.348 652 8823	0.000 760 1409	0.290 285 7298
$17f_1-f_b$	37.601 712 0341	0.000 956 0414	0.661 809 7441
$17f_1-2f_b$	37.582 719 6786	0.000 794 0197	0.445 059 0258
$18f_1-f_b$	39.815 878 4185	0.000 971 0316	0.149 495 683
$18f_1-2f_b$	39.795 046 2168	0.000 747 7844	0.094 751 1938

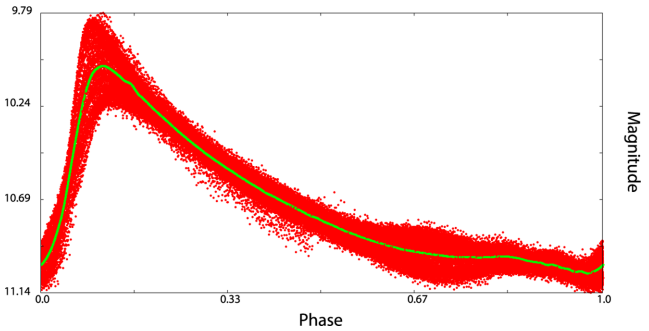

Figure 9. Folded light curve with main pulsation $f_1 = 2.213\,027\,17$ d^{-1} (in red); PDM mean curve (in green).

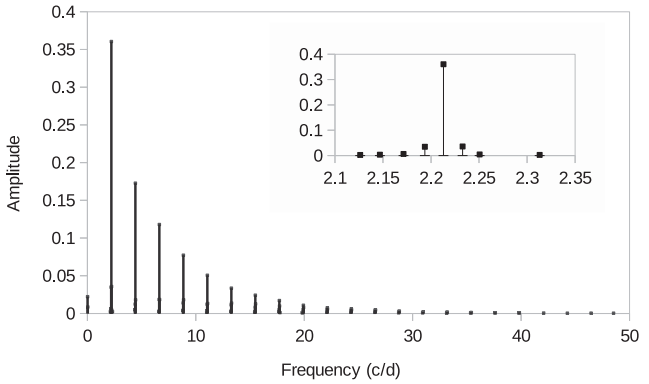

Figure 10. Frequency spectrum of S Arae. The insert panel shows the multiplet structure around the main frequency.

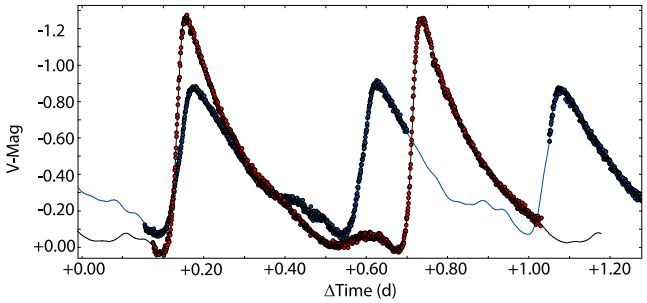

Figure 11. S Arae light curve at minimum – blue – and maximum – red – Blazhko cycle. The two parts were superposed to compare the amplitude, period and shape change of the light curve between the minimum and maximum Blazhko phase.

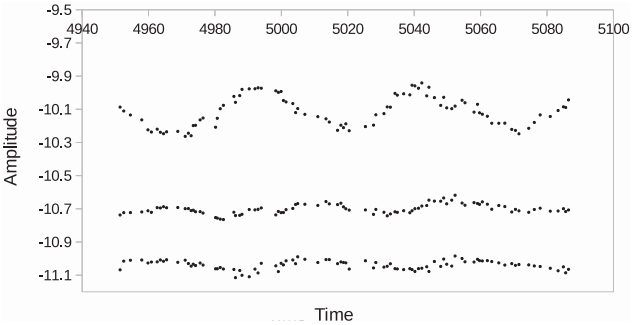

Figure 12. Maximum (top), mean (middle) and minimum (bottom) representation of the light-curve envelope.

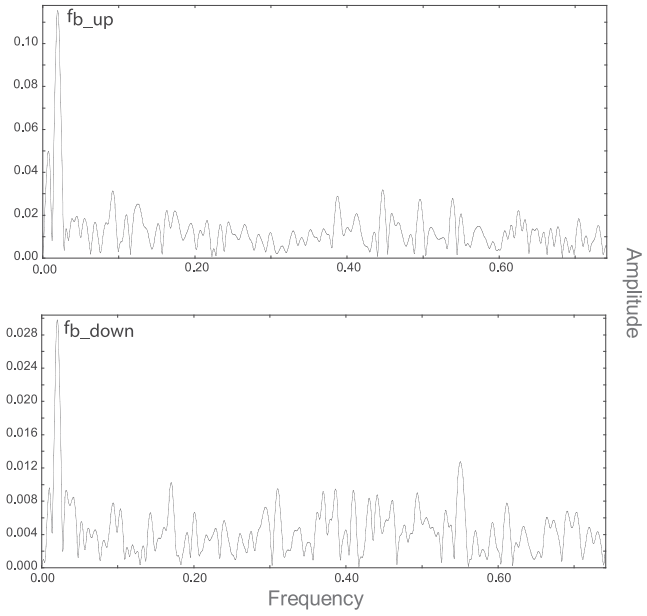

Figure 13. Top: original spectrum of the upper part of the modulation envelope. Bottom: original spectrum of the lower part of the modulation envelope.

Blazhko cycle to another – occurring earlier in the second one. More observations, including several Blazhko cycle is necessary to infer our hypothesis. R_{21} amplitude ratio also presents an oscillatory behaviour, although less obvious than A_1, with constant subset when A_1 reaches its maximum value. These two oscillations have an

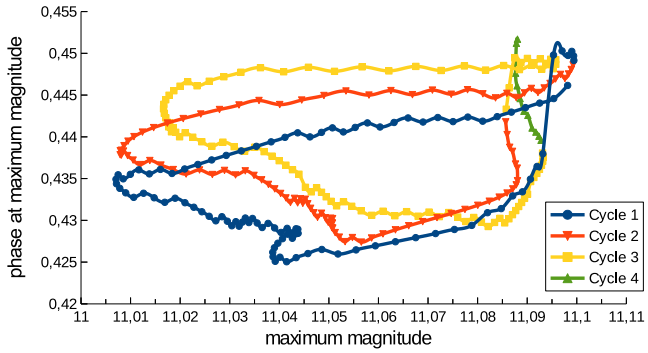

Figure 14. Maximum magnitude phase against maximum magnitude for each pulsation period along three Blazhko cycles of S Arae.

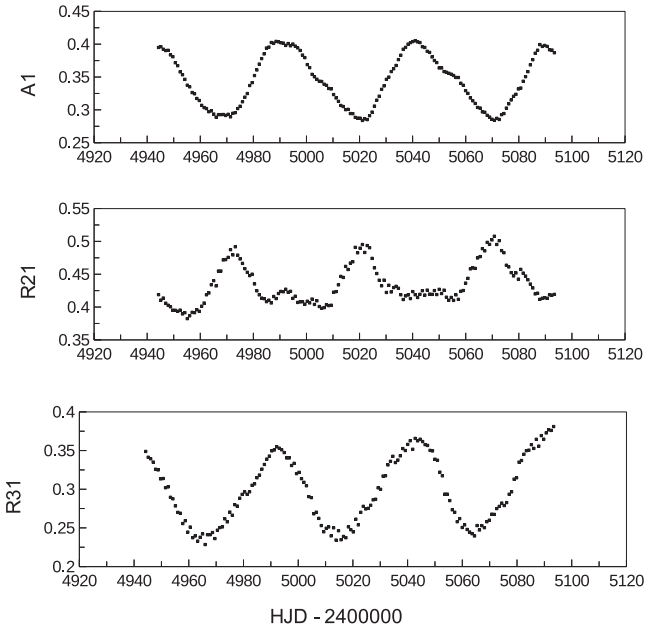

Figure 15. Evolution of the amplitude Fourier parameters during the three Blazhko cycles, calculated for two periods bins. From top to bottom: fundamental frequency Fourier amplitude A_1, amplitude ratio R_{21} and R_{31}.

Table 8. Average epoch-independent Fourier parameters of S Arae.

Parameter	Value	Parameter	Value
A_1	0.345	ϕ_1	3.016
R_{21}	0.434	ϕ_{21}	3.890
R_{31}	0.298	ϕ_{31}	6.723

approximate π radians phase difference, while A_1 and R_{31} can be considered in phase.

Other binning – modification of the time span and/or overlap – gave similar results leading to the conclusion that the influence of the bin structure was limited.

3.2.4 *Rise time*

Fig. 16 presents the evolution of the rise time along the total time span of three modulation cycles. The overall evolution is very similar to A_1 variation that we commented in last paragraph. We can clearly see that the Blazhko effect affects also the dynamic of the star as the rise time decreases when reaching maximum magnitude in the Blazhko cycle. Besides the moving bump perturbation observed precedently repeats here near the minimums.

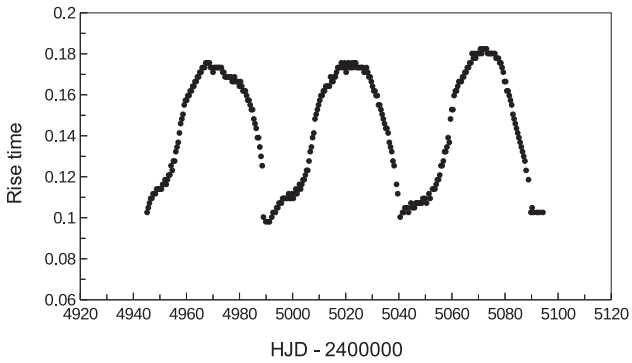

Figure 16. Variation of the rise time during the three Blazhko cycles.

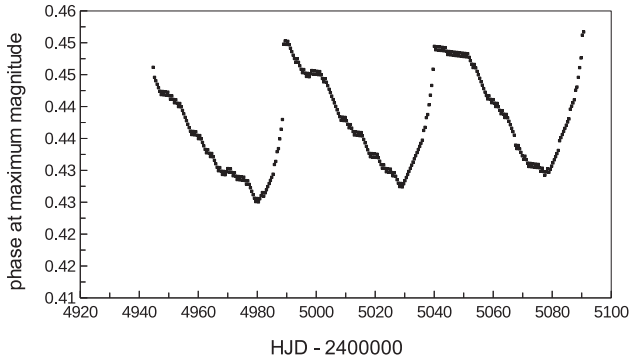

Figure 17. Variation of the maximum magnitude phase for each pulsation period.

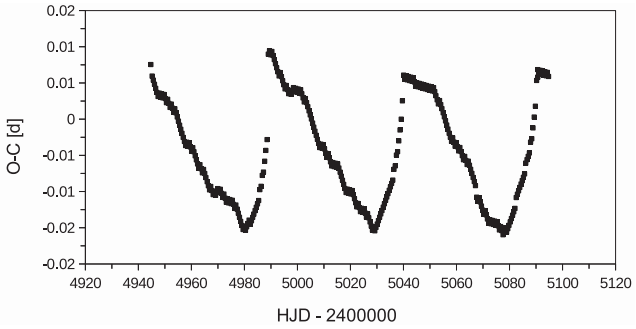

Figure 18. O−C diagram of the total data set for S Arae.

3.2.5 *O−C diagram*

In addition to the maximum magnitude–maximum phase plot (Fig. 17), the O−C diagram is a complementary tool to investigate phase modulation. Indeed, the O−C diagram is primarily intended for the investigation of period changes by comparing, the timing of an event with the expected time of occurrence, according to a constant periodicity. In the case of Blazhko stars, we use it to detect period changes which are seemingly caused by phase modulation.

We worked with an epoch value $T_0 = 245039.1498$ HJD and a pulsation period $P_0 = 0.4519$ d. The plot obtained (Fig. 18) is, as expected, very similar to the maximum magnitude–maximum phase, exhibiting a clear periodic period change due to the phase modulation.

Table 9. Comparison of metallicities obtained for different Blazhko phase, according to, respectively, equations (7), (5) and (8).

$\Delta\Phi$	$A_{\rm tot}$	$[Fe/H]_{A_{\rm tot}}$	ϕ_{31}	$[Fe/H]_{\phi_{31}}$	RT	$[Fe/H]_{\rm RT}$	$\langle[Fe/H]\rangle$	$\Delta_{A-\phi_{31}}$	$\Delta_{A-{\rm RT}}$	$\Delta_{{\rm RT}-\phi_{31}}$	$\sigma_{[Fe/H]}$
0.0–0.1	1.31	−1.30	4.12	−2.23	0.13	−0.43	−1.32	0.94	0.87	1.81	0.74
0.1–0.2	1.22	−1.16	2.74	−4.17	0.16	−0.45	−1.93	3.02	0.71	3.73	1.62
0.2–0.3	1.07	−0.95	1.58	−5.81	0.17	−0.37	−2.38	4.87	0.58	5.45	2.44
0.3–0.4	0.98	−0.81	0.77	−6.96	0.17	−0.35	−2.71	6.14	0.46	6.61	3.01
0.4–0.5	0.93	−0.74	3.70	−2.83	0.17	−0.37	−1.31	2.09	0.37	2.46	1.08
0.5–0.6	1.02	−0.87	3.64	−2.91	0.16	−0.43	−1.40	2.04	0.45	2.48	1.08
0.6–0.7	1.07	−0.94	4.85	−1.21	0.14	−0.55	−0.90	0.27	0.39	0.66	0.27
0.7–0.8	1.21	−1.15	2.82	−4.06	0.12	−0.69	−1.97	2.91	0.46	3.37	1.49
0.8–0.9	1.31	−1.30	5.12	−0.82	0.11	−0.76	−0.96	0.48	0.54	0.06	0.24
0.9–1.0	1.33	−1.32	5.88	0.26	0.11	−0.76	−0.61	1.59	0.56	1.02	0.66

4 FUNDAMENTAL PARAMETERS AND DISCUSSION

4.1 Physical characteristics

A good synthesis of the available formulae to compute physical characteristics of RRab stars can be found in Nemec (2011). However, these equations do not suit well to amplitude and phase-modulated stars (Nemec et al. 2013) because the input parameters (ϕ_{31}, A_V, etc.), as we saw in the previous section, vary over a Blazhko period. Different approaches have been considered to resolve this issue. The first one consisted in taking the values obtained from the analysis of the whole data set. This lead to values of metallicity [Fe/H] ranging from −2.31 to −0.5, which made this method inconsistent. The second approach relied on the parameters derived from the unmodulated signal. After gathering all significant frequencies from the analysis of the whole survey, we removed the multiplet structure, Blazhko period and harmonics, and fitted the remaining frequencies with the original data. The values obtained were similar to those of the modulated signal, hence leading to the same conclusion. The third approach averaged the Fourier parameters extracted from 10 phase bins, i.e. 0–0.1, 0.1–0.2, etc. The results, once again led to similar discrepancies. Finally, we considered that the equations intended for non-Blazhko stars could be applied to Blazhko stars but only when the latter were in a specific phase. Thus we computed the metallicity, for which we have four different equations, involving three varying parameters (ϕ_{31}, A_V and rise time) for each of the 10 bins described above, and look for results with low discrepancy and plausible values. More details on the formulae can be found in the next paragraph. The results confirmed our intuition, with one bin (0.6–0.7) showing consistent values for [Fe/H].[1] Table 9 sums up all the values obtained for [Fe/H] regarding the different method exposed.

4.1.1 *Metal abundances*

Four methods have been used to estimate metal abundances. Each of these are based on, or derived from, Oosterhoff (1939), Arp (1955) and Preston (1959) period–amplitude diagram. The additional equations come from Kovács & Walker (2001) and Sandage (2004) work using the correlation between ϕ_{31}, rise time and amplitude. All results are summarized in Tables 9 and 10.

Two [Fe/H] scales are used in the following discussion: the Zinn and West metallicity scale (Zinn & West 1984), noted $[Fe/H]_{\rm ZW}$ hereafter; the Butler–Blanco (Sandage 2004) and Caretta and Gratton (Carretta & Gratton 1997) scales which are similar, noted $[Fe/H]_{\rm BB}$ or $[Fe/H]_{\rm CG}$. These scales are linked by the equation $[Fe/H]_{\rm ZW} = 1.05[Fe/H]_{\rm CG} - 0.20$ giving the CG-scale a metallicity of ≈0.2 dex more than the ZW-scale (Jurcsik 1995).

Metal abundance based on log P–ϕ_{31}–[Fe/H] relations: the lines of constant $[Fe/H]_{\rm CG}$ in the period–ϕ_{31} diagram are given by (Jurcsik 1998)

$$[Fe/H]_{\rm CG} = -5.038 - 5.394P + 1.345\phi_{31}. \quad (5)$$

Sandage (2004) gave a second estimate of [Fe/H] based on an $[Fe/H]_{\rm ZW}$–log P–ϕ_{31} relation:

$$[Fe/H]_{\rm ZW} = 1.411\phi_{31} - 7.012\log P - 6.025, \quad (6)$$

where ϕ_{31} is the Fourier phase parameter for a cosine fit, which differs by π radians with the one derived from a sine fit: $\phi^{\rm c}_{31} = \phi^{\rm s}_{31} - 3.141\,59$ (using 's' and 'c' superscripts for phase parameters computed with, respectively, sine and cosine series). The $\phi^{\rm c}_{31}$ and the log P coefficients have, respectively, uncertainties of ±0.014 and ±0.071. Metallicities derived from equations (5) and (6) are listed in Table 10 under, respectively, $\phi^{\rm s}_{31}$ and $\phi^{\rm c}_{31}$.

Metal abundance based on log P–$A_{\rm tot}$–[Fe/H] relations: metallicity can also be evaluated using the period–amplitude relation given by Sandage 2004

$$[Fe/H]_{\rm ZW} = -1.453A_{\rm tot} - 7.990\log P - 2.145, \quad (7)$$

where the error for each coefficient is ±0.027, ±0.091 and ±0.043 dex, respectively. The result is listed in Table 10 under $A_{\rm tot}$. This equation was the one used in Feast et al. (2008) to compute the existing value of [Fe/H] for S Arae. The value used for $A_{\rm tot}$ was based on an average of $A_{\rm tot}$ obtained for each period of the available observations. As we have seen in the beginning of this section, this approach leads to biased results, and therefore needs to be reconsidered.

Metal abundance based on log P–RT–[Fe/H] relations: finally, the last estimate of [Fe/H] can be obtained from the period–rise time diagram using the Sandage (2004) relation

$$[Fe/H]_{\rm ZW} = 6.33{\rm RT} - 9.11\log P - 4.60. \quad (8)$$

The result is listed in Table 10 under RT.

Table 10. Metal abundances derived from the pulsation period relation with Fourier phase parameter, amplitude and rise time.

$\phi^{\rm s}_{31}$	$\phi^{\rm c}_{31}$	[Fe/H] $A_{\rm tot}$	RT	Adopted	log Z ($\alpha = 0$)
−1.21	−1.20	−0.94	−0.55	−0.90 (0.27)	−2.67

[1] To support our argument, Appendix A presents another example of Blazhko star, MW Lyr, for which this method was applied successfully.

Table 11. Physical characteristics of S Arae.

$(B-V)_0$		M_V				$T_{\rm eff}$	log g		L(puls)		L(evol)			M(puls)		M(evol)	
J98	KW01	J98	F98	B07	C08	KW01	J98	KW99	J98	J98	S06	S06	S06	J98	J98	S06	B07
0.310	0.304	0.91	0.93	0.81	0.78	6743	2.896	2.872	34.3	32.95	37.35	38.72	43.35	0.51	0.52	0.60	0.62

Adopted metallicity: as discussed by Nemec (2011), systematic discrepancies are seen between each of these four methods. Usually, the methods based on ϕ_{31} give similar results while the one based on the rise time gives higher metallicity than the others. Therefore, we averaged the values obtained with equations (5), (7) and (8) for the 0.6–0.7 phase, to compute the adopted metallicity. Table 10 gives the averaged estimate with its standard deviation in parentheses. The uncertainty on [Fe/H] is slightly higher (0.27 dex) than the averaged 0.17 standard deviation observed by Nemec over 19 RRab stars. The 0.8–0.9 would have also been a good candidate considering its standard deviation. However, the small standard deviation comes mostly from the quasi-similar values obtain with the methods based on rise time and ϕ_{31} while the discrepancies between the other methods are larger than the one obtained with the 0.6–0.7 phase. Hence our choice for this latter interval. Finally, the fourth column of Table 10 gives log Z, which differs from [Fe/H] by log $Z_\odot$ where $Z_\odot = 0.017\,16$ (Sweigart & Catelan 1998), assuming [α/Fe] = 0.

4.1.2 Reddenings and Mean Colours

Dereddened colours: the dereddened mean $B-V$ colour can be calculated using period P and Fourier A_1 coefficient (Jurcsik 1998) –

$$(B-V)_0 = 0.308 + 0.163P - 0.187A_1. \quad (9)$$

Another equation is given by Kovács & Walker (2001) which includes the A_3 Fourier coefficient:

$$(B-V)_0 = 0.189 \log P - 0.313A_1 + 0.293A_3 + 0.460. \quad (10)$$

Both results are listed in column 1 of Table 11 under, respectively, J98 and KW01. As both are very similar, we will adopt the average of the two colour estimates 0.307 in the following analysis.

Reddenings and extinctions: *E(B−V)* reddenings derived from the large-scale reddening maps of Schlegel, Finkbeiner and Davis (Schlegel, Finkbeiner & Davis 1998) can be found in Table 12 column 4. The results were obtained using DUST and the galactic coordinates given in Table 12 columns 2 and 3. Assuming an extinction to reddening ratio $A_V/E(B-V) = 3.1$, the total extinction in the V passband, A_V, was calculated and given in column 5 of Table 12.

4.1.3 Effective temperatures

Considering the $(B-V)_0$ found in last paragraph, effective temperature was estimated using the Kovács & Walker (2001) formulae supposing [α/H] = 0:

$$\log T_{\rm eff} = 3.8840 - 0.3219(B-V)_0 + 0.0167 \log g + 0.0070[{\rm Fe/H}]_{\rm CG}. \quad (11)$$

Estimate is available in column 3 of Table 11 under KW01.

4.1.4 Absolute magnitudes

Jurcsik (1998) gave a first equation for absolute magnitude based on A_1 and ϕ_{31}:

$$M_V = 1.221 - 1.396P - 0.477A_1 + 0.103\phi_{31}. \quad (12)$$

The result is listed in column 3 of Table 11 under J98. A second estimate of M_V is the Fernley et al. (1998) equation:

$$M_V = 0.18[{\rm Fe/H}]_{\rm CG} + 1.05, \quad (13)$$

assuming that RR Lyr has $M_V = 0.78(\pm 0.29)$ at $[{\rm Fe/H}]_{\rm CG} = -1.39$ dex. The uncertainties are ± 0.03 on the [Fe/H] coefficient and ± 0.2 on the other coefficient. The result is in column 2 of Table 11 under F98. In general these M_V values are similar, with a mean difference of only $0.01(\pm 0.01)$ mag.

According to Bono, Caputo & Di Criscienzo (2007), for galactic field variables with metallicities included in the −2.5 to 0 dex range, the absolute magnitude can be obtained using

$$M_V = 1.19 + 0.5[{\rm Fe/H}]_{\rm ZW} + 0.09[{\rm Fe/H}]^2_{\rm ZW}. \quad (14)$$

The result is listed in column 3 of Table 11 under B07.

Finally, a fourth estimate of M_V was given recently by Catelan & Cortés (2008):

$$M_V = 0.23[{\rm Fe/H}]_{\rm ZW} + 0.984. \quad (15)$$

The result is listed in column 3 of Table 11 under C08. On average, absolute magnitude obtained with this last equation are ≈0.15 mag brighter than the F98 and B07 values (Nemec 2011) and those in turn are ≈0.05 mag brighter than the J98 value. Still, M_V standard deviation of 0.07 mag for these four values correspond to the 0.20 mag uncertainty in the individual estimate. The average absolute magnitude obtained over these four results is 0.86 mag.

4.1.5 Distance

Table 12 column 8 contains the approximate distance of S Arae, computed using M_V, $<V>$ and the visual extinction given in column 5 of the same table.

Table 12. Observational characteristics of S Arae.

$\langle V \rangle$ (mag)	l (°)	b (°)	$E(B-V)$ (mag)	A_V (mag)	$(B-V)_0$ J98	$(B-V)_0$ KW01	d (kpc)
10.70	343.3792	−12.4479	0.15 (0.003)	0.46	0.310	0.304	1.2

Considering an uncertainty of ≈0.01 mag for m_V, of ≈0.07 mag for M_V and of ≈0.01 mag for A_V, the distance calculated is given with a precision of about 100 pc.

4.1.6 Surface gravities

To calculate the mean surface gravity we used equation 15 from Jurcsik (1998) and equation 12 from Kovács & Walker (2001). The first one depends only on the period and is given by

$$\log g = 2.473 - 1.226 \log P. \quad (16)$$

The second one depends on mass, period and effective temperature:

$$\log g = 2.938 + 0.230 \log M - 0.110 \log T_{\rm eff} - 1.219 \log P. \quad (17)$$

Estimates are given in column 4 of Table 11 under J98 and KW99.

4.1.7 Luminosities and masses

To derive luminosity and mass, two methods can be applied: the pulsational method and the evolutionary method. The first one is derived from Albada and Baker equations (van Albada & Baker 1971, 1973) which links the pulsation period to mass, luminosity and $T_{\rm eff}$ – this being also derived from the basic von Ritter equation of stellar pulsation $P\sqrt{\rho} = Q$, where ρ is the mean density in cgs and Q is the pulsation constant. The second method is based on stellar evolutionary models which describes the evolution of luminosity and effective temperature of a zero-age horizontal branch star with a given input mass M and chemical composition (X, Y, Z). Existing models are those by Dorman (1992), Bono et al. (1997) and VandenBerg et al. (2000).

Pulsational L and M: pulsational luminosity can be computed using two equations. Both are given by Jurcsik (1998). The first one depends only on the metallicity and the result is given in column 5 of Table 11:

$$\log L = 1.464 - 0.106[{\rm Fe/H}]_{\rm CG}. \quad (18)$$

The second depends on metallicity and effective temperature:

$$\log L = 10.260 - 0.062[{\rm Fe/H}]_{\rm CG} - 2.294 \log T_{\rm eff}. \quad (19)$$

Similarly, pulsational mass can be calculated *via* two formulae (Jurcsik 1998):

$$\log M = 1.477 \log L - 1.754 \log P + 0.037[{\rm Fe/H}]_{\rm CG} - 6.272 \log T_{\rm eff} + 20.884 \quad (20)$$

$$\log M = -0.328 - 0.062[{\rm Fe/H}]_{\rm CG}. \quad (21)$$

Results are displayed in column 8 of Table 11.

L and M from stellar evolution models: following the Caputo et al. (2000) stellar evolution models, Sandage (2006) gave a first equation for $L_{\rm (evol)}$ as a function of [Fe/H] –

$$\log L = 1.245 - 0.451[{\rm Fe/H}]_{\rm ZW} - 0.097[{\rm Fe/H}]^2_{\rm ZW}. \quad (22)$$

The second equation is based on Catelan, Pritzl & Smith (2004) alpha-enhanced zero-age horizontal branch model:

$$\log L = 1.404 - 0.243[{\rm Fe/H}]_{\rm ZW} - 0.043[{\rm Fe/H}]^2_{\rm ZW}. \quad (23)$$

The third one, derived from Clementini et al. (2003), differs from the previous one as it does not assume a quadratic dependence on [Fe/H]:

$$\log L = 1.538 - 0.110[{\rm Fe/H}]_{\rm ZW}. \quad (24)$$

Results are displayed in column 7 of Table 11. As pointed out by Nemec in his study of several ab-type RR Lyrae star observed by the Kepler telescope (Nemec 2011), L(evol) are systematically larger than L(puls). Besides, the results are also consistent with the fact that stars with high metallicity are less luminous than metal-poor stars.

Mass can be obtained using the Bono et al. (1997) model as shown by Sandage (2006):

$$\log M = -0.283 - 0.066[{\rm Fe/H}]_{\rm ZW}. \quad (25)$$

Another way to compute it was given by Bono et al. (2007) based on the Pietrinferni et al. horizontal branch model (Pietrinferni et al. 2004, 2006):

$$\log M = -0.2675 - 0.063[{\rm Fe/H}]_{\rm ZW}. \quad (26)$$

Results are available in column 9 of Table 11. Similarly to what we observed for the luminosity, M(evol) values are larger than M(puls).

4.2 Shock waves and bump dynamics

As described by Chadid et al. (2014), the light curve is noticeably distorted by shock waves. The bump, occurring before the light-curve minimum, is associated with the shock wave $Sh_{\rm PM3}$ resulting from the collision of the infalling atmosphere with the expanding photosphere. According to their study and following the Stellingwerf work (Stellingwerf 2013), the multishock structure could be responsible for the Blazhko effect as it develops a stationary coronal structure that drives an outflowing wind.

4.2.1 Residual light curve and shock waves

Fig. 19 shows the residual light curve after pre-whitening the main pulsation, the Blazhko period and the sidelobes of each multiplet, in an attempt to remove the Blazhko modulation from the data set. The most striking feature of the residual light curve is the intense variation that appears around phase 0.9 in a narrow 10 per cent phase interval of the pulsation cycle. Chadid et al. (2014) have pointed out that this variation is a consequence of a strong shock wave, named $Sh_{\rm H+He}$, traversing the photosphere of S Arae and created by the κ and γ mechanisms during the rise time of the light curve. Such strong shock wave is at the origin of the 'hump' observed just before the light-curve maximum (Chadid 2000; Chadid & Preston 2013). A similar residual scatter was observed in near the light-curve maxima of the Blazhko star DR Andromedea (Lee & Schmidt 2001) and the Blazhko star RR Gem (Jurcsik et al. 2005) occurring in a phase interval of 20 per cent of the pulsation cycle, twice larger than the case of S Arae – meaning that the main shock is stronger in S Arae than in those stars.

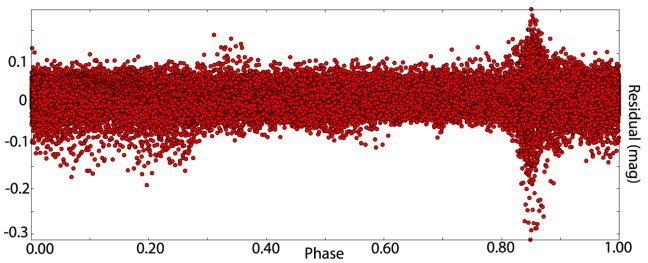

Figure 19. Residual light curve after pre-whitening with the main pulsation, the Blazhko period and sidelobe frequencies.

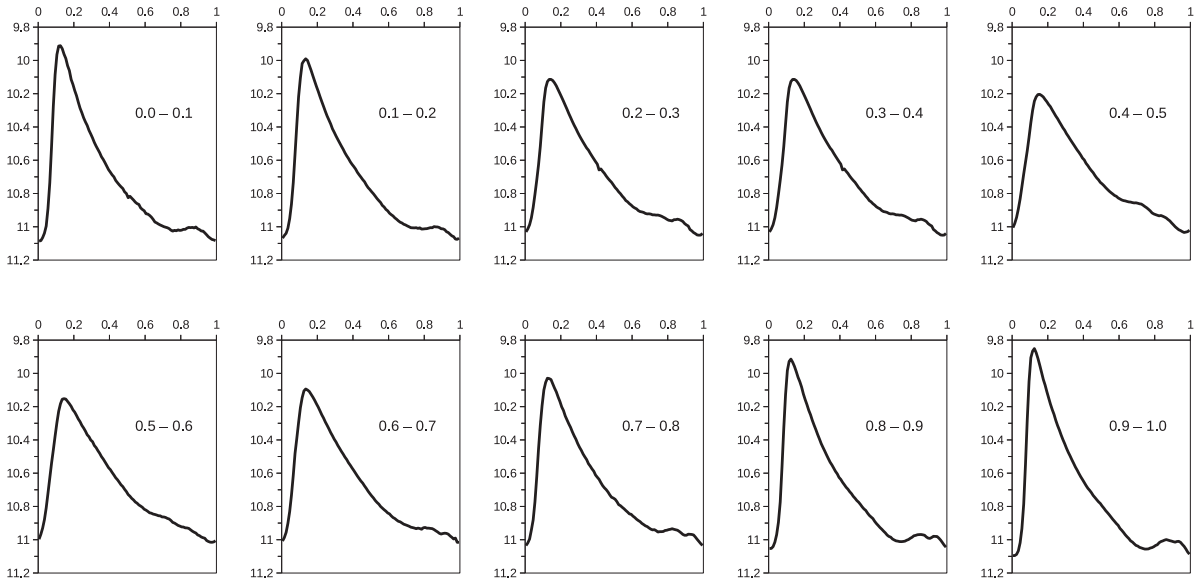

Figure 20. Bump evolution during the Blazhko cycle.

4.2.2 Bump dynamics

The bump position in a given RR Lyrae can change from one Blazhko phase to another (Chadid et al. 2011). PDM mean curve (Fig. 9, green curve) is particularly interesting in that regard. The bump is not as clear as it can be seen in Fig. 20 at phase $\psi = 0$ for instance. On the contrary, we have a quasi-smooth line, confirming the idea of a non-stationary process. After subdividing the data in 10 bins according to the Blazhko period–phase diagram, we have plotted the mean light curve folded with the mean period for each of these 10 bins (Fig. 20).

First, the topology of the bump is quite unusual. In fact, there is not a single bump but one main bump surrounded by two others which appear and vanish depending on the Blazhko phase. Indeed, from phase $\psi = 0.20$ to 0.50 a second bump appears before the main one, but soon vanishes to let a new second bump appear after the initial peak from phase $\psi = 0.60$ to 0.90.

Moreover, it appears that the central peak, which is the only one visible at $\psi = 0.10$, has a 0.05 phase span, varying from 0.81 to 0.86 and therefore, suggests a possible link between the Blazhko phenomenon and the dynamics of the bump.

Knowing that the main bump undergoes a phase variation, it could be possible that the two surrounding bumps are in fact just one bump which also presents a phase variation. Indeed, as described above, the surrounding bumps are not both visible at a given phase. Hence, the secondary peak observed after the main bump between $\psi = 0.60$ and 0.90, may just be the one observed from $\psi = 0.20$ to 0.50 which underwent a phase translation. This means that the main bump would have a 5 per cent phase variation and the secondary one a 20 per cent phase variation.

5 CONCLUSIONS

The unique Antarctica PAIX data, with its high time sampling, high optical photometric precision and long time base of 150 d, allowed us to disclose new results about the RR ab Blazhko star S Arae. The frequency analysis was performed using both Period04 and PDM13; three significant frequencies corresponding to two non-radial modes and a plausible radial overtone were extracted. The main pulsation exhibits an asymmetric multiplet structure, amplitude and frequency wise, and we also suggested that the main pulsation harmonics follow a hyperbolic decrease rather than an exponential one. We were able to compute the physical parameters of the star, using a new approach to avoid the difficulties faced when studying properties of Blazhko-type star and finding a medium metallicity for S Arae. Finally, we studied the multishock structure before the light-curve minimum, and show that the bump distortion was in fact composed of one quasi-static main bump, which undergoes a 5 per cent phase variation, and a more peculiar secondary bump which had a 20 per cent phase variation, moving from one side of the main bump to another during a Blazhko cycle.

ACKNOWLEDGEMENTS

We thank the US Air Force Research Laboratory, Agence Nationale de la Recherche (ANR-OS-BLAN-0033-01), Conseil des Programmes Scientifiques et Technologiques (CPST) for their great support. We would also like to thank the Polar Institut Paul Emile Victor (IPEV) for the precious infrastructure and friendly help. M. Chadid is indebted to all the people who participated in the Antarctica expeditions within the PAIX framework.

REFERENCES

Alcock C. et al., 2003, ApJ, 598, 597
Arp H. C., 1955, AJ, 60, 317
Benkő J. M., Szabó R., Paparó M., 2011, MNRAS, 417, 974
Blazko S., 1907, Astron. Nachr., 175, 327
Bono G., Caputo F., Cassisi S., Incerpi R., Marconi M., 1997, ApJ, 483, 811
Bono G., Caputo F., Di Criscienzo M., 2007, A&A, 476, 779
Buchler J. R., Kolláth Z., 2011, ApJ, 731, 24
Caputo F., Castellani V., Marconi M., Ripepi V., 2000, MNRAS, 316, 819
Carretta E., Gratton R. G., 1997, A&AS, 121, 95
Catelan M., Cortés C., 2008, ApJ, 676, L135
Catelan M., Pritzl B. J., Smith H. A., 2004, ApJS, 154, 633

Chadid M., 2000, A&A, 359, 991
Chadid M., Chapellier E., 2006, A& A, 456, 305
Chadid M., Preston G. W., 2013, MNRAS, 434, 552
Chadid M., Wade G. A., Shorlin S. L. S., Landstreet J. D., 2004, A&A, 413, 1087
Chadid M. et al., 2010a, A&A, 510, A39
Chadid M., Vernin J., Mekarnia D., Chapellier E., Trinquet H., Bono G., 2010b, A&A, 516, L15
Chadid M., Perini C., Bono G., Auvergne M., Baglin A., Weiss W. W., Deboscher J., 2011, A&A, 527, A146
Chadid M. et al., 2014, AJ, 148, 88
Clementini G., Gratton R., Bragaglia A., Carretta E., Di Fabrizio L., Maio M., 2003, AJ, 125, 1309
Dorman B., 1992, ApJS, 81, 221
Dziembowski W. A., Cassisi S., 1999, Acta Astron., 49, 371
Feast M. W., Laney C. D., Kinman T. D., van Leeuwen F., Whitelock P. A., 2008, MNRAS, 386, 2115
Fernley J., Barnes T. G., Skillen I., Hawley S. L., Hanley C. J., Evans D. W., Solano E., Garrido R., 1998, A&A, 330, 515
Guggenberger E., Kolenberg K., 2006, Commun. Asteroseismology, 148, 21
Guggenberger E. et al., 2012, MNRAS, 424, 649
Hertzsprung E., 1926, Bull. Astron. Inst. Neth., 3, 115
Hill S. J., 1972, ApJ, 178, 793
Jurcsik J., 1995, Acta Astron., 45, 653
Jurcsik J., 1998, A&A, 333, 571
Jurcsik J. et al., 2005, A&A, 430, 1049
Jurcsik J. et al., 2008, MNRAS, 391, 164
Jurcsik J. et al., 2009, MNRAS, 393, 1553
Kovács G., Walker A. R., 2001, A&A, 374, 264
Lee A. F. S., Heghinian M., 1977, Technometrics, 19, 503
Lee K. M., Schmidt E. G., 2001, PASP, 113, 1140
Lenz P., Breger M., 2005, Commun. Asteroseismology, 146, 53
Linnell Nemec A. F., Nemec J. M., 1985, AJ, 90, 2317
Molnár L., Kolláth Z., Szabó R., 2012, MNRAS, 424, 31
Nemec J. M. et al., 2011, MNRAS, 417, 1022
Nemec J. M., Cohen J. G., Ripepi V., Derekas A., Moskalik P., Sesar B., Chadid M., Bruntt H., 2013, ApJ, 773, 181
Nowakowski R. M., Dziembowski W. A., 2001, Acta Astron., 51, 5
Oosterhoff P. T., 1939, Observatory, 62, 104
Pietrinferni A., Cassisi S., Salaris M., Castelli F., 2004, ApJ, 612, 168
Pietrinferni A., Cassisi S., Salaris M., Castelli F., 2006, ApJ, 642, 797
Popielski B. L., Dziembowski W. A., Cassisi S., 2000, Acta Astron., 50, 491
Poretti E. et al., 2010, A&A, 520, A108
Preston G. W., 1959, ApJ, 130, 507
Sandage A., 2004, AJ, 128, 858
Sandage A., 2006, AJ, 131, 1750
Schlegel D. J., Finkbeiner D. P., Davis M., 1998, ApJ, 500, 525
Schwarzenberg-Czerny A., 1997, ApJ, 489, 941
Shibahashi H., 2000, in Szabados L., Kurtz D., eds, ASP Conf. Ser. Vol. 203, IAU Colloq. 176: The Impact of Large-Scale Surveys on Pulsating Star Research. Astron. Soc. Pac., San Francisco, p. 299
Simon N. R., Lee A. S., 1981, ApJ, 248, 291
Smolec R., Moskalik P., 2008, Acta Astron., 58, 193
Sódor Á., Jurcsik J., Szeidl B., 2009, MNRAS, 394, 261
Stellingwerf R. F., 1978, ApJ, 224, 953
Stellingwerf R. F., 2011, in McWilliam A., ed., RR Lyrae Stars, Metal-Poor Stars, and the Galaxy. The Observatories of the Carnegie Institution of Washington, Pasadena, CA, p. 47
Stellingwerf R. F., 2013, preprint (arXiv:1310.0535)
Stothers R. B., 2006, ApJ, 652, 643
Sweigart A. V., Catelan M., 1998, ApJ, 501, L63
Szabó R., 2014, in Guzik J. A., Chaplin W. J., Handler G., Pigulski A., eds, Proc. IAU Symp. 301, Precision Asteroseismology. Cambridge Univ. Press, Cambridge, p. 241
Szabó R., Kolláth Z., Buchler J. R., 2004, A&A, 425, 627
Szabó R. et al., 2010, MNRAS, 409, 1244
van Albada T. S., Baker N., 1971, ApJ, 169, 311
van Albada T. S., Baker N., 1973, ApJ, 185, 477
Van Hoolst T., Dziembowski W. A., Kawaler S. D., 1998, MNRAS, 297, 536
VandenBerg D. A., Swenson F. J., Rogers F. J., Iglesias C. A., Alexander D. R., 2000, ApJ, 532, 430
Zalian C., Chadid M., Stellingwerf R. F., 2014, MNRAS, 440, 68
Zinn R., West M. J., 1984, ApJS, 55, 45

APPENDIX A: MW LYRAE METALLICITY USING THE PHASE METHOD

MW Lyrae is a Blazhko RR Lyrae-type star with a 0.3976 d period and a 16.5462 d modulation period. An exhaustive study of MW Lyr is available in Jurcsik et al. (2008) and Jurcsik et al. (2009). They have found an [Fe/H] value ranging between −0.4 and −0.6. Fixing its value to −0.5, they then computed the physical parameters of the star using the IP method (Sódor, Jurcsik & Szeidl 2009). We applied the method described in Section 4 to compute MW Lyr metallicity. Table A1 presents the results computed for each of the 10 bins using equations (5), (7) and (8). The best candidate is the 0.5–0.6 phase with a $\sigma_{[Fe/H]}$ value of 0.36. The amplitude and ϕ_{31} equations give a metallicity which corresponds to the range given by Jurcsik et al. The one obtained with the rise time equation shows a noticeable discrepancy which cause $<[Fe/H]>$ to deviate from the $[-0.4;-0.6]$ interval expected. However, Table A1 shows clearly that none of the bins, expect the one selected, lead to relevant results, confirming our method.

Table A1. Comparison of metallicities obtained for different Blazhko phase, according to, respectively, equations (7), (5) and (8) for MW Lyrae.

$\Delta\Phi$	A_V	$[Fe/H]_{A_V}$	ϕ_{31}	$[Fe/H]_{\phi_{31}}$	RT	$[Fe/H]_{RT}$	$<[Fe/H]>$	$\Delta_{A-\phi_{31}}$	Δ_{A-RT}	$\Delta_{RT-\phi_{31}}$	$\sigma_{[Fe/H]}$
0.0–0.1	1.39	−1.41	3.32	−3.35	0.17	0.27	−1.50	1.94	1.69	3.63	1.48
0.1–0.2	1.39	−1.41	3.82	−2.66	0.18	−0.33	−1.47	1.25	1.07	2.32	0.95
0.2–0.3	1.24	−1.20	4.06	−2.32	0.22	−0.09	−1.20	1.12	1.11	2.23	0.91
0.3–0.4	1.00	−0.85	2.59	−4.39	0.25	0.16	−1.69	3.54	1.00	4.55	1.95
0.4–0.5	0.89	−0.68	3.92	−2.51	0.27	0.24	−0.98	1.83	0.91	2.74	1.14
0.5–0.6	0.81	−0.57	5.43	−0.38	0.27	0.27	−0.22	0.18	0.84	0.65	0.36
0.6–0.7	0.78	−0.52	1.94	−5.31	0.30	0.42	−1.80	4.79	0.94	5.72	2.51
0.7–0.8	0.91	−0.70	0.98	−6.66	0.28	0.30	−2.36	5.96	1.00	6.96	3.07
0.8–0.9	1.13	−1.03	3.95	−2.47	0.22	−0.09	−1.20	1.44	0.94	2.37	0.98
0.9–1.0	1.31	−1.29	0.60	−7.21	0.17	−0.38	−2.96	5.92	0.91	6.83	3.03

This paper has been typeset from a TEX/LATEX file prepared by the author.